Title
Ground Motion Intensity Measures at Liquefaction Field Case History Sites

Journal
Journal of Geotechnical and Geoenvironmental Engineering, 152(8)

ISSN
1090-0241

Authors
Pretell, Renmin
Brandenberg, Scott J
Stewart, Jonathan P

Publication Date
2026-08-01

DOI
10.1061/jggefk.gteng-14212

Peer reviewed

This is the authors' final version of the manuscript, and is not the official version. It is being shared as an open source alternative to the official published version of the manuscript, which can be found at the link below.

https://doi.org/10.1061/JGGEFK.GTENG-14212

Ground Motion Intensity Measures at Liquefaction Field Case History Sites

Renmin Pretell, Ph.D., M. ASCE[1], Scott J. Brandenberg, Ph.D., P.E., M. ASCE[2], and Jonathan P. Stewart, Ph.D., P.E., F. ASCE[3]

[1] Assistant Professor, Dept. Civil & Environ. Eng., Univ. of Nevada, Reno, 1664 N. Virginia St., Reno, NV 89557-0258, email: rpretell@unr.edu (Corresponding author)

[2] Professor, Dept. Civil & Environ. Eng., Univ. California, Los Angeles, 405 Hilgard Avenue, Los Angeles, CA 90095 1593, email: sjbrandenberg@g.ucla.edu

[3] Professor, Dept. Civil & Environ. Eng., Univ. California, Los Angeles, 405 Hilgard Avenue, Los Angeles, CA 90095 1593, email: jstewart@seas.ucla.edu

Abstract

The state of practice for assessing soil liquefaction triggering relies on semi-empirical models that use the peak ground acceleration (*PGA*) at the ground surface and the earthquake magnitude (**M**) to represent the seismic demand leading to liquefaction or lack thereof. Analysts have used various methods to compute *PGA*s at liquefaction case history sites from past earthquakes. *PGA* was often taken as equal to the value recorded at the nearest seismic station, sometimes adjusted based on the results of one-dimensional (1D) ground response analyses to account for differences in site effects. Ground motion models or judgment were often used when a site was not located near a seismic station. These approaches do not account for the differences in path effects between the liquefaction site and the nearest ground motion recording, may neglect differences in site conditions between a seismic station and a liquefaction site, and do not generally consider *PGA* spatial correlation. This paper's objective is to compute *PGA*s at 569 case history sites in the Next Generation Liquefaction (NGL) database using a consistent approach that builds on previous studies. Three alternative intensity measures (*IM*s) are also computed at the liquefaction sites, namely peak ground velocity (*PGV*), Arias intensity (I_A), and cumulative absolute velocity (*CAV*). A comparison of legacy and newly estimated *PGA*s indicates a mean difference of -0.034 in natural logarithmic units (legacy values larger) and 95% of our values lie between 55 to 180% (i.e., a factor of 1.8) of legacy *PGA*s. This shows that the previous and new *PGA* values are

comparable as a whole, but individual cases have appreciable differences, the causes of which are explained in this paper.

Introduction

The state of practice for assessing soil liquefaction triggering relies on models developed based on field case histories. These databases consist of ground failure cases that manifested at the surface due to liquefaction, and non-ground failure cases at sites where liquefaction might have reasonably been anticipated (e.g., Seed and Idriss 1971, Cetin et al. 2000, Youd et al. 2001, Cetin et al. 2004, Moss et al. 2006, Boulanger and Idriss 2014, Cetin et al. 2018). A key component of these case histories is the seismic demand at the case history sites. Traditionally, this seismic demand is represented by cyclic stress ratio (*CSR*), adjusted both for a reference earthquake magnitude of **M** = 7.5 and for a vertical effective stress σ_v' = 1 atm ($CSR_{M=7.5,\sigma_v'=1}$), as defined in Eq. 1 (Idriss and Boulanger 2008).

$$CSR_{\boldsymbol{M}=7.5,\sigma_v'=1} = 0.65 \cdot \frac{PGA}{g} \cdot \frac{\sigma_v}{\sigma_v'} \cdot r_d \cdot \frac{1}{MSF} \cdot \frac{1}{K_\sigma} \quad (1)$$

where *PGA* is the peak ground acceleration at the ground surface, g is the acceleration of gravity in the same units as *PGA*, σ_v is the in-situ vertical total stress, σ_v' is the in-situ vertical effective stress, r_d is a depth reduction factor, *MSF* is the magnitude scaling factor, and K_σ is an overburden correction factor. Additional correction factors can be applied to account for the influence of static shear stress. Estimating a suitable *PGA* is an important consideration when using Eq. 1 to evaluate liquefaction case histories or for forward applications.

Various methods for estimating *PGA* are summarized in Table 1 and are listed in order of decreasing accuracy based on our judgment. Method 1 involves a ground motion instrument collocated with a liquefaction observation and is deemed the most accurate. However, collocated recordings are often affected by factors such as shaking-induced excess porewater pressure and dilation-induced acceleration spikes, and thus their direct use in triggering model development is not straightforward (Özener et al. 2020). The next best is interpolation of residuals from a grid of measured ground motions, as done in Method 2 and often Method 3. Method 2, interpolating within-event residuals, is preferred to direct interpolation of *IM*s because *IM*s are not spatially stationary and differences in site conditions are addressed when interpreting within-event residuals. Method 2 is distinct from post-earthquake ground motion maps (Method 3), such as the versions of U.S. Geological Survey (USGS) ShakeMaps produced shortly following major earthquakes, because the goal of those maps is to produce near real-time indicators of shaking intensity, which means that the level of care adopted in ground motion processing is less rigorous. Moreover, some maps are based on estimations or correlations with macroseismic intensity. Modern USGS ShakeMaps use a similar Kriging-interpolation approach as the one presented in this work (e.g., Worden et al. 2018, Engler et al. 2022), and therefore Methods 2 and 3 are conceptually similar. When updated after careful ground motion processing and human review, ShakeMaps should be considered equivalent to Method 2.

Table 1. Summary of methods used to estimate ground motion intensity measures (*IM*s) in legacy datasets.

Method	Description	Comment
1	Recorded at the site, collocated	Direct measurements at location of interest.
2	Interpolated from recordings at nearby stations	Interpolation is conducted on within-event residuals.
3	Near real-time post-earthquake maps	Post-earthquake ground motion maps based on recorded shaking intensities and interpolation of ground motion intensity measures.
4	Based on ground response analyses	Advantageous for sites with strong impedance contrasts, but uncertainty in the input motion makes this method less favorable.
5	Recorded at the nearest seismic station	Relatively common in past practice, but seismic stations are often several kilometers from a liquefaction site.
6	Based on ground motion models	High uncertainty because both between- and within-event variability apply in the absence of recorded event-specific ground motions.
7	Based on judgment	Not well documented, difficult to reproduce.

One-dimensional (1D) ground response analysis (Method 4) can be accurate at sites with deep shear-wave velocity (V_S) profiles containing strong impedance contrasts, and where the motion can be reasonably estimated below the impedance contrast (e.g., the "rock" motion). However, even in cases where a nearby rock outcrop motion is recorded, the recording is seldom close enough for the rock motion to be characteristic of the incident motion at the site. Method 5 was relatively common in past practice, in which analysts adopted the *PGA* recorded at the nearest seismic station. In many cases, that nearest seismic station was several kilometers away from the site, thus significant differences in *PGA* values may arise from differing path and site effects. Method 4 often used input motions obtained using Method 5 and therefore inherits some of its uncertainty. Method 6 uses ergodic ground motion models (GMMs), which carry a high degree of uncertainty because, in the absence of event-specific recordings, both between- and within-event sources of variability contribute to the uncertainty of ground motion estimates. Method 7 estimates *PGA*s based on judgment. These judgments were often not well documented and are difficult to reproduce. Therefore, we consider Method 7 to be the least preferred method. The variety of methods used to develop *PGA* estimates in legacy models leads to (1) *IM*s that are inconsistent with *IM*s derived in forward analyses, which are generally estimated using probabilistic seismic hazard analysis (PSHA), and (2) *IM*s that in some cases are biased, mainly due to inadequate consideration of path and site effects. These inconsistencies, in turn, might limit the predictive ability of liquefaction triggering models.

Liquefaction datasets and models have predominantly used *PGA* and **M** to quantify the seismic demand leading to soil liquefaction, but there is potential for using other ground motion *IM*s to characterize demand. For instance, Kayen and Mitchell (1997) proposed a liquefaction triggering procedure that uses Arias intensity (I_A) to represent seismic demand. Kramer and Mitchell (2006) evaluated several ground motion *IM*s for their efficiency, sufficiency and predictability. They found that the cumulative absolute velocity (*CAV*) estimated for ground motion time series with an acceleration cutoff of 5 cm/s^2 (CAV_5) is a good predictor of excess porewater pressure ratio (r_u) and thus liquefaction triggering. Kramer and Sideras (2022) proposed a ground motion *IM*, denoted IM_L, based on observations from cyclic direct simple shear tests conducted with transient, irregular loading. The authors found that IM_L can account for the ground motion duration and amplitude effects on soil liquefaction. These and other studies suggest a potential for ground motion *IM*s other than *PGA* to increase the predictive ability of semi-empirical liquefaction triggering models.

Ground motion interpolation (i.e., Methods 2 and 3) requires an understanding of the spatial correlation of shaking intensity. Ground motions attenuate with distance from the fault rupture and are therefore non-stationary. Common methods of interpolation, such as ordinary Kriging (Krige 1951), assume a stationary random field. For this reason, interpolation is generally performed on within-event residuals because the ground motion model removes many non-stationary effects. Spatial correlation of within-event residuals arises from unmodeled source, path, and site effects. For example, the amount of slip is not constant along a fault, and ground motions tend to be stronger near high slip zones and smaller near low slip zones. These variations are not captured by the input parameters used in most GMMs. Similarly, site response may differ from GMM predictions due to strong impedance contrasts, basin edge effects, or topographic amplification effects that are not captured by the time-averaged shear wave velocity in the upper 30m (V_{S30}), or isosurface depth parameters (e.g., $z_{1.0}$, $z_{2.5}$). These geologic features tend to be spatially correlated due to the underlying geologic processes that formed them, and the within-event residuals therefore inherit this spatial correlation. Path effects may also contribute to spatial correlation of within-event residuals due to spatial variability in crustal attenuation (e.g., Kuehn et al. 2019). Spatial correlation of within-event residuals therefore consists of event-specific components, such as the fault slip distribution and the path between the fault rupture and site, and sub-regionally persistent features, such as site response effects and crustal attenuation patterns. The sub-regional properties could conceivably be quantified, thereby reducing uncertainty in spatial correlation of within-event residuals for forward applications, such as probabilistic seismic hazard analysis. However, this paper focuses on event-specific spatial correlation of within-event residuals, which is influenced by source, path, and site effects. Event-specific spatial correlation relationships cannot be generalized to future, unrealized events, but provide the most accurate interpolation strategy for individual events that are well recorded.

In this study, we compute the mean and uncertainty of *PGA*s of case history sites in the Next Generation Liquefaction (NGL) database (Brandenberg et al. 2020, Ulmer et al. 2023) using a framework that builds on previous studies. In addition to *PGA*, we also apply the framework to compute peak ground velocity (*PGV*), I_A, and *CAV*. Previous studies that used a framework similar to that presented here for different applications include Kwak et al. (2012), Stafford (2012), Bradley (2014), Worden et al. (2018), and Engler et al. (2022); an important new element of the present work is event-specific customization of spatial variability models using Bayesian methods, as detailed subsequently. Following this introduction, we first present the data resources that were used, including ground motion measurements and liquefaction site information. The methodology used to interpolate ground motions at liquefaction sites is then described, including the calculation of event terms and within-event residuals, the development of correlation models using Bayesian inference, and spatial interpolation. The legacy *PGA*s (i.e., those used in past triggering models), and the newly estimated *PGA*s are then compared. We conclude by investigating the impact of the new *PGA*s on liquefaction triggering relationships. Preliminary versions of the work presented here appear in conference papers and a report (Hudson et al. 2023, Pretell et al. 2024a, 2024b).

Data resources

Data resources used in this study are contained in the NGL database (Ulmer et al. 2023) and the Next Generation Attenuation (NGA) databases, NGA-West2 (Ancheta et al. 2014), NGA-Sub (Mazzoni et al. 2022), and NGA-East (Goulet et al. 2021). Spatial interpolation is much more accurate when neighboring ground motion recordings are available. For this reason, we added ground motion recordings that are not included in NGA products at a few key locations (e.g., the Watsonville recording for the Loma Prieta event downloaded from the Center for Engineering

Strong Motion Data, CESMD). These added recordings mainly include ground motions from other databases, single-component recordings that may have been screened for NGA applications, and *IM*s reported in the literature. We disregarded collocated ground motion recordings that were affected by soil liquefaction, as identified by Özener et al. (2020), except for three cases where we considered the ground motions to be usable because liquefaction triggered late in the record. We also disregarded four recorded *PGA*s of the **M**6.2 Christchurch Earthquake identified to be affected by dilation spikes and instead used the *PGA*s recommended by Upadhyaya et al. (2019). Details of the non-NGA ground motions used herein are provided by Pretell et al. (2024b). The data used in this study consist of (1) 8,424 ground motion recordings with event and path metadata and (2) locations and site investigation data for 569 sites from 46 earthquakes in the NGL database where observations of liquefaction or lack thereof were made following one or more earthquakes. Fig. 1 is an example map for the 1989 **M**6.9 Loma Prieta Earthquake of available recordings and the NGL (i.e., case history) sites where ground motions are to be estimated.

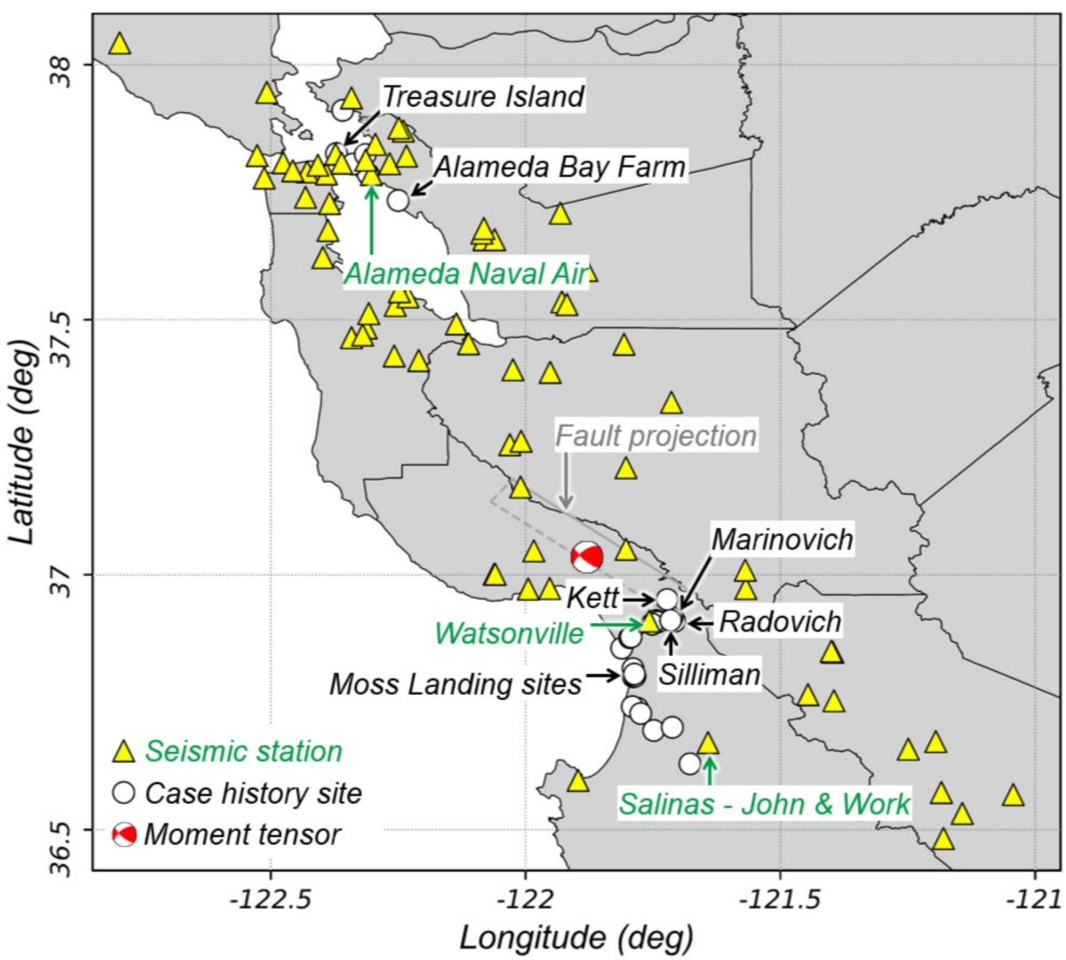

Fig. 1. Map of seismic stations that recorded the 1989 **M**6.9 Loma Prieta Earthquake.

An important site parameter is the time-averaged V_S in the upper 30 m of the site (V_{S30}) because GMMs use it to estimate site response. For seismic station locations, we used V_{S30} values from previously published NGA sources (Seyhan et al. 2014, Goulet et al. 2021, Ahdi et al. 2022). For NGL sites, we computed V_{S30} from V_S measurements when available and otherwise used correlations with penetration resistance from cone penetration tests (CPTs) or standard penetration tests (SPTs). The correlations proposed by Hegazy and Mayne (2006), Andrus et al. (2007), and Robertson (2012) were used to estimate V_{S30} based on CPT data and were averaged with equal weight given to each model. For sites in New Zealand, the region-specific correlation by McGann et al. (2015) was used. The correlation by Brandenberg et al. (2010) was used to estimate V_{S30} based on SPT data. When both CPT and SPT data were available, a weighted average V_{S30} was computed, using weights of 2 and 1 for CPT- and SPT-based V_{S30} values, respectively. In addition, a weight inversely proportional to the distance from the CPT or SPT to the site location was applied. The site location was selected as the centroid of all the associated CPT and SPT locations, which is considered appropriate given the likely negligible variation in ground motion *IM*s within an area spanning a few tens of meters. In cases where V_S profiles were available to depths exceeding 30 m, V_{S30} was computed directly. In cases where the V_S profile extends to a depth shallower than 30 m, an extrapolation to 30 m was conducted based on Boore (2004).

A minimum V_{S30} of 150 m/s was used to compute ground motions at case history sites with V_{S30} lower than 150 m/s. This minimum value was used because (1) ergodic GMMs are not calibrated for values lower than around 150 m/s, thus the use of values lower than 150 m/s would represent an uncontrolled extrapolation that may produce unrealistic site response estimates, and (2) recent studies demonstrate saturation effects at low V_S values (e.g., Buckreis et al. 2024). Of 418 unique NGL sites in our dataset, 16% (66 sites) have a V_{S30} lower than 150 m/s. These sites correspond to case histories from 10 events in New Zealand (7 events), Japan (2 events), and Türkiye (1 event).

Methodology

The methodology for interpolating ground motion *IM*s at liquefaction sites consists of ordinary Kriging interpolation of within-event residuals. The following subsections describe the procedures adopted to compute within-event residuals, develop spatial correlation models, and perform Kriging interpolation.

Total residuals and event terms

The total *IM* residuals for an earthquake event i recorded at a seismic station j (δ_{ij}) were calculated as the difference between the recorded *IM* (Y_{ij}), and the mean *IM* estimated using a GMM ($\mu_{\hat{Y}_{ij}}$), as indicated in Eq. 2.

$$\delta_{ij} = ln(Y_{ij}) - ln\left(\mu_{\hat{Y}_{ij}}\right) \quad (2)$$

The uncertainty associated with the GMM selected for computing $\mu_{\hat{Y}}$ is addressed by using multiple GMMs, selected based on the tectonic region according to Table 2. Additional information on GMM selection is provided subsequently in this paper.

Table 2. Ground motion models used for computing ground motion intensity measures.

Tectonic setting	Ground motion *IM* [1]	Ground motion model
Active Crustal	*PGA* and *PGV*	Abrahamson et al. (2014)
Active Crustal	*PGA* and *PGV*	Boore et al. (2014)
Active Crustal	*PGA* and *PGV*	Campbell and Bozorgnia (2014)
Active Crustal	*PGA* and *PGV*	Chiou and Youngs (2014)
Active Crustal	I_A and *CAV*	Campbell and Bozorgnia (2019)
Subduction	*PGA*	Abrahamson and Gülerce (2022)
Subduction	*PGA* and *PGV*	Kuehn et al. (2023)
Subduction	*PGA* and *PGV*	Parker et al. (2022)
Subduction and active crustal earthquakes (sites in Japan)	I_A and *CAV*	Foulser-Piggott and Goda (2015)
Stable continental	*PGA* and *PGV*	Goulet et al. (2021)
Stable continental	I_A and *CAV*	Farhadi and Pezeshk (2020)

[1] *PGA*: Peak ground acceleration, *PGV*: peak ground velocity, I_A: Arias intensity, *CAV*: cumulative absolute velocity.

The event term for event i ($\eta_{E,i}$) was approximated as the mean total residual across seismic stations j using Eq. 3.

$$\eta_{E,i} \approx \sum_{j=1}^{N_{rec,i}} w_j \cdot \delta_{ij} \quad (3)$$

where w are weights computed from the station-to-station covariance matrix as discussed in the next paragraph, and N_{rec} is the number of recordings available for event i. Event terms computed in this manner differ from those computed in GMMs, as GMMs derive event terms based on mixed-effects regressions (e.g., Abrahamson and Youngs 1992). However, this approach has the favorable feature of being applicable to any event, not only to those included in GMM development datasets.

The weights in Eq. 3 account for the spatial distribution of recording stations to obtain an unbiased estimation of the event term. For example, if two collocated stations produce identical ground motions, using both with equal weight to other motions would constitute double-counting, and would bias the event term estimation. To this end, the weights are computed considering the correlation amongst the seismic stations to prevent data redundancy. The weights are equal to the top N_{rec} elements of the right-most column of the inverse of the augmented covariance matrix (**C**), obtained by appending a column and a row of ones (and a zero) to **C**, as shown in Eq. 4.

$$w_j = \left[\begin{pmatrix} \boldsymbol{C} & \mathbf{1} \\ \mathbf{1}^T & 0 \end{pmatrix}^{-1}\right]_{j,N_{rec}+1} \tag{4}$$

where **C** is derived for each station-to-station pair. In essence, Eq. 4 is a simplification of the ordinary Kriging equation, with the particularity that the cross-covariance matrix between the sampled and unsampled locations is zero. The covariance matrix for the seismic stations, **C**, is defined based on spatial correlation models, described later. The event term does not impact the computed ground motion *IM*s as we remove it and add it back after Kriging, to recover the ground motion estimate at a point. However, the event term does influence the within-event residual values, and event terms used herein are always consistent with the event-specific correlation model.

The uncertainty in η_E is represented by a normally distributed random variable with zero mean, and standard deviation τ. In forward PSHA applications, no information is available about the event term, so τ from the GMM should be used to estimate event term uncertainty. In contrast, when an event has occurred and produced ground motion recordings, the event term uncertainty is reduced but not fully eliminated because of sampling error, which decreases as N_{rec} increases. The standard error of the sampling distribution for an event i ($\bar{\tau}_i$) is provided by Eq. 5, where τ_i is the between-event standard deviation given by GMMs.

$$\bar{\tau}_i = \frac{\tau_i}{\sqrt{N_{rec,i}}} \tag{5}$$

Within-event residuals

Within-event residuals for a given event i at a seismic station j (δW_{ij}) are computed by subtracting the event term, using Eq. 6.

$$\delta W_{ij} = \delta_{ij} - \eta_{E,i} \tag{6}$$

The δW_{ij} values were then normalized using Eq. 7 for consistency with the approach to develop correlation models by Bodenmann et al. (2023), where $\delta \widehat{W}_{ij}$ is the normalized within-event residual, and ϕ_i is the standard deviation of δW computed from the data using Eq. (6).

$$\delta \widehat{W}_{ij} = \frac{\delta W_{ij}}{\phi_i} \tag{7}$$

Examples of δW are presented in Fig. 2 (indicated by the color at the seismic station locations) for the 1989 **M**6.9 Loma Prieta Earthquake, developed for *PGA* estimates ($\hat{Y}_{ij}$) based on the Boore et al. 2014 (BSSA14) GMM. The map shows that the within-event residuals are spatially correlated, with a cluster of positive values in the central Bay Area (including the Treasure Island and Alameda Bay Farm stations indicated in Fig. 2) and clusters of negative values closer to the southern end of the fault rupture.

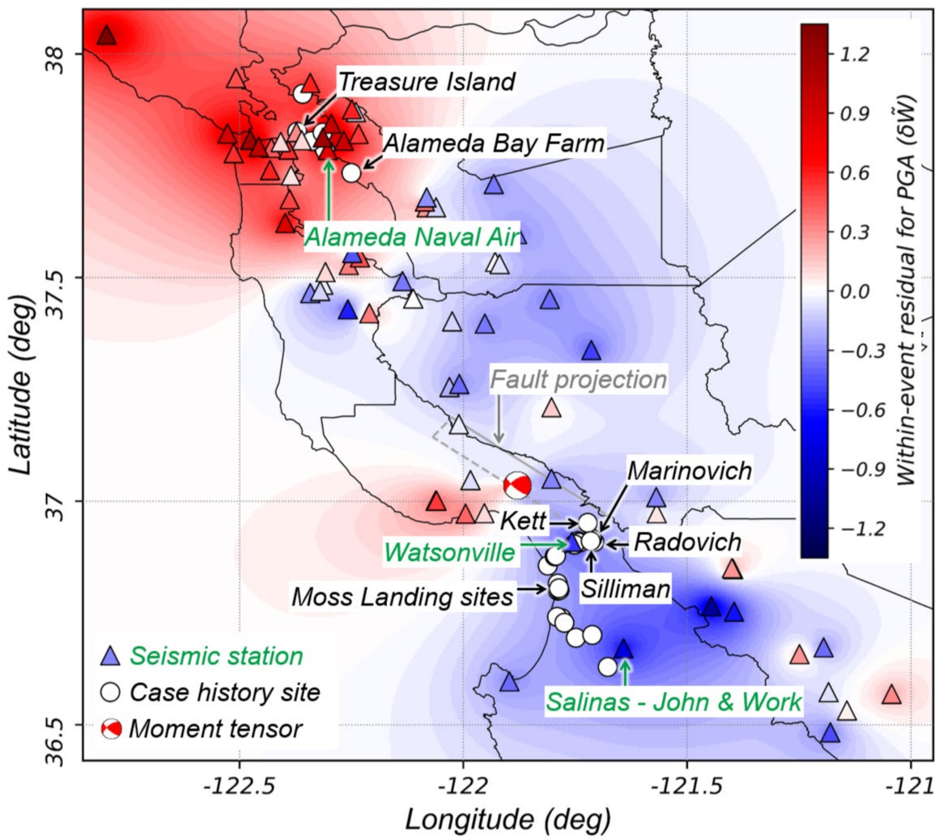

Fig. 2. Map of mean interpolated *PGA* within-event residuals for the 1989 **M**6.9 Loma Prieta Earthquake using the maximum a posteriori correlation model.

Spatial correlation models

Kriging interpolation requires a spatial correlation model describing the correlation of a random variable between the measurement and interpolation points. Some earthquakes are recorded by a dense seismic network, and a correlation model can be derived empirically from the recordings. In other cases, ground motion recordings are scarce and widely spaced, and the number of recordings is inadequate to resolve a statistically robust data-driven correlation model. We adopted the "EA" correlation model functional form developed by Bodenmann et al. (2023) in which correlation is a function of Euclidean separation distance (d_E), and epicenter-to-site azimuth (d_A), as defined by Eq. 8,

$$\rho_{EA} = exp\left[-\left(\frac{d_E}{\ell_E}\right)^{\gamma_E}\right] \cdot \left(1 + \frac{d_A}{\ell_A}\right)\left(1 - \frac{d_A}{180°}\right)^{180°/\ell_A} \tag{8}$$

where γ_E is an exponent coefficient that controls the shape of the correlation function, ℓ_E is the Euclidean correlation length, and ℓ_A is the azimuthal correlation length. Bodenmann et al. (2023) also proposed a model for the spatial correlation due to site effects (denoted "EAS"), however, the authors indicated that site effects had only a minor influence on spatial correlation for long-oscillator period spectral accelerations.

The data used in the spatial correlation analyses are identical to those used in residuals analyses, with the exception that data were only considered up to the cutoff distances in Table 3. The reason for this screen was so that the resulting models would apply for relatively near-field conditions where most liquefaction case histories are located. Similar to Bodenmann et al. (2023), we used Bayesian inference to draw 1000 samples from the posterior distributions of the model coefficients for each event. To this end, we used the PyMC Python library (Salvatier et al. 2016) and the No U-Turn Sampler to draw samples. The prior distributions for the model coefficients used by Bodenmann et al. (2023) were adopted herein and subsequently updated on an event-specific basis. Bodenmann et al. (2023) did not study *PGV*, I_A, or *CAV*. However, they used the same prior distributions for spectral accelerations at oscillator periods ranging from 0.01 to 6 seconds. Similarly, we used the same prior distributions for each parameter. Though not presented here for brevity, the prior distributions by Bodenmann et al. (2023) were observed to bound the range of *PGA* correlation models for geologically variable, and geologically similar conditions suggested by Jayaram and Baker (2009). Samples of the model coefficients for the Loma Prieta event are presented in Fig. 3. Correlation models for well-recorded events are essentially data-driven, with little influence from the prior distributions and narrow posterior distributions, whereas correlation models for poorly recorded events are influenced by the prior distributions and have broader distributions of model coefficients. Posterior distributions of the model coefficients constitute a source of epistemic uncertainty in the spatial correlation model that is incorporated into the estimates of the ground motion *IM*s, as described later.

Table 3. Maximum distance per tectonic setting for the derivation of spatial correlation models.

Tectonic setting	Distance cutoff [1]
Active crustal	$R_{JB} < 50$ km
Subduction	$R_{rup} < 200$ km
Stable continental	$R_{rup} < 500$ km

[1] R_{JB}: Joyner-Boore distance, R_{rup}: rupture distance.

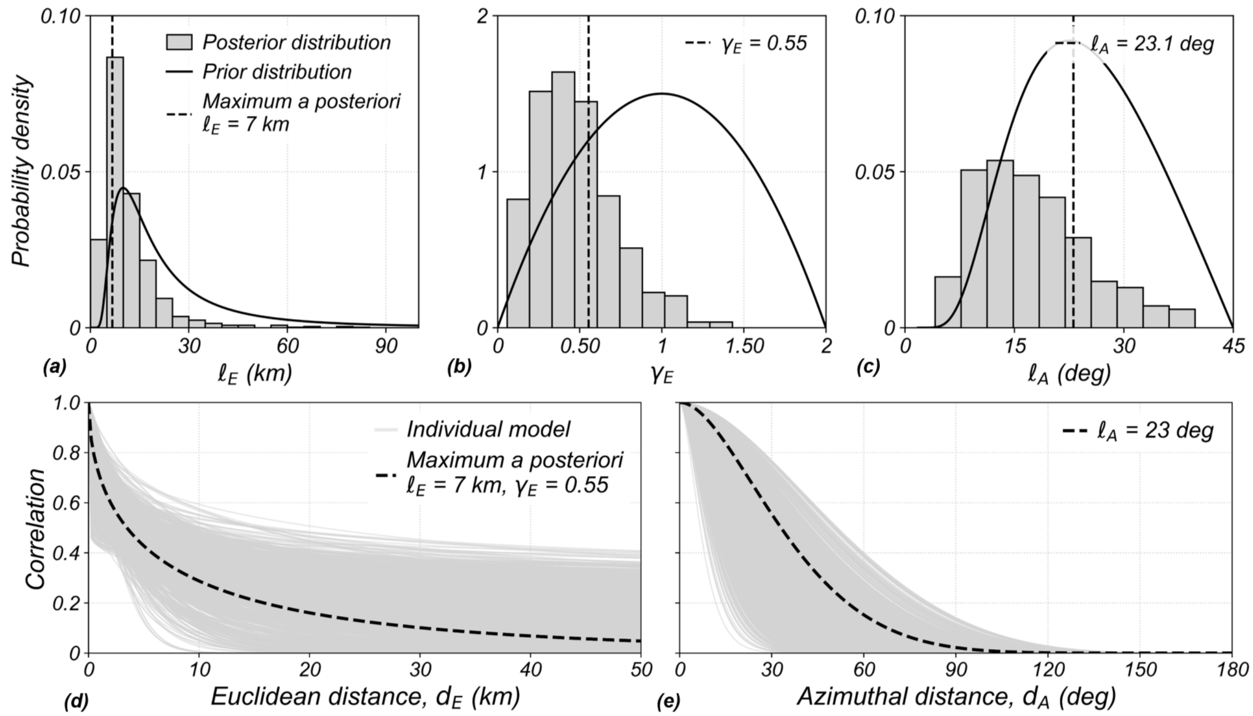

Fig. 3. Posterior samples of spatial correlation models of *PGA* within-event residuals for the 1989 **M**6.9 Loma Prieta Earthquake.

Interpolation of ground motion intensity measure within-event residuals

We interpolated within-event residuals ($\delta\widetilde{W}$) at NGL sites using ordinary Kriging (Krige 1951). We conducted Kriging interpolation using all the available measured ground motions to obtain a mean within-event residual, $\mu_{\delta\widetilde{W}}$, and its standard deviation, $\sigma_{\delta\widetilde{W}}$, at the locations of NGL case histories. The elements of the covariance matrix, **C**, between ground motion recording stations were computed using Eq. 9,

$$C_{mn} = (\phi^2 + \bar{\tau}^2) \cdot \rho_{EA,mn} \tag{9}$$

where m and n denote seismic station indices, ϕ is the standard deviation of δW defined by the GMM, $\bar{\tau}$ is the standard deviation of the event-specific event term defined by Eq. 5, and $\rho_{EA,mn}$ is the correlation coefficient between the seismic station and NGL locations between seismic stations *m* and *n*, computed from Eq. 8. Similarly, a cross-covariance matrix was computed between the ground motion recording stations and the interpolation locations (i.e., NGL sites).

Eq. 9 reflects our belief that GMMs should reasonably constrain the variance at large separation distances. The ϕ and τ values were selected for a condition representative of NGL sites, i.e., **M**7, Joyner-Boore distance (R_{JB}) of 50 km for crustal active regions, rupture distance (R_{rup}) of 100 km for subduction regions, and V_{S30} of 200 m/s. For the single case history in a continental region, ϕ and τ depend on earthquake magnitude alone and were selected for a **M**5 event. Tables 4 and 5 summarize the ϕ and τ values selected by tectonic setting.

Table 4. Within- (ϕ) and between-event (τ) standard deviations representative of NGL sites in different tectonic settings: Peak ground acceleration (*PGA*) and peak ground velocity (*PGV*).

Tectonic setting [1]	Ground motion model	Abbreviation	*PGA*		*PGV*	
			ϕ	τ	ϕ	τ
Active crustal	Abrahamson et al. (2014)	ASK14	0.477	0.311	0.509	0.378
Active crustal	Boore et al. (2014)	BSSA14	0.472	0.346	0.604	0.239
Active crustal	Campbell and Bozorgnia (2014)	CB14	0.445	0.274	0.478	0.280
Active crustal	Chiou and Youngs (2014)	CY14	0.451	0.224	0.444	0.231
Subduction (interface)	Abrahamson and Gülerce (2022)	AG22	0.525	0.331	-	-
Subduction (intraslab)	Abrahamson and Gülerce (2022)	AG22	0.510	0.310	-	-
Subduction	Parker et al. (2022)	PSBAH22	0.465	0.480	0.411	0.477
Subduction	Kuehn et al. (2023)	KBCG23	0.596	0.489	0.511	0.451
Stable continental	Goulet et al. (2021)	Gea21	0.620	0.417	0.604	0.353

[1] ϕ and τ selected for **M**7, R_{JB} = 50 km, and V_{S30} = 200 m/s (active crustal region); **M**7, R_{rup} = 100 km, and V_{S30} = 200 m/s (subduction region), and **M**5 (stable continental region).

Table 5. Within- (ϕ) and between-event (τ) standard deviations representative of NGL sites in different tectonic settings: Arias intensity (I_A), and cumulative absolute velocity (*CAV*).

Tectonic setting [1]	Ground motion model	Abbreviation	I_A		*CAV*	
			ϕ	τ	ϕ	τ
Active crustal	Campbell and Bozorgnia (2019)	CB19	0.762	0.372	0.359	0.207
Subduction	Foulser-Piggott and Goda (2015)	FPG15	1.035	0.901	0.490	0.411
Stable continental	Farhadi and Pezeshk (2020)	FP20	1.270	0.820	0.610	0.410

[1] ϕ and τ selected for **M**7, R_{JB} = 50 km, and V_{S30} = 200 m/s (active crustal region); **M**7, R_{rup} = 100 km, and V_{S30} = 200 m/s (subduction region), and **M**5 (stable continental region).

Calculation of means and uncertainties of ground motion intensity measures

The mean value for a ground motion *IM* ($\mu_{\bar{Y}}$) for earthquake event i at a NGL site j calculated using a spatial correlation model k developed based on a GMM ℓ can be defined in Eq. 10:

$$\mu_{\tilde{Y},ijk\ell} = \mu_{\hat{Y},ij\ell} + \eta_{E,i\ell} + \mu_{\delta\widetilde{W},ijk\ell} \tag{10}$$

Eq. 10 represents the basic elements of the proposed approach, which is that the mean ground motion *IM* estimate $\mu_{\tilde{Y}}$ (in natural logarithmic units) is the sum of the mean GMM prediction ($\mu_{\hat{Y}}$), the event term η_E, and the location-specific estimate of the mean within-event residual $\mu_{\delta\widetilde{W}}$ from Kriging interpolation. In the absence of ground motion measurements, which is the case for some older earthquakes, no Kriging interpolation was conducted, and Eq. 10 reduces to $\mu_{\tilde{Y},ij\ell} = \mu_{\hat{Y},ij\ell}$. This reduced version of Eq. 10 is used for 79 NGL sites from 14 events, which represent 14% of the NGL case histories. Case histories with ground motion measurements at a distance large enough that the spatial correlation ρ_{EA} is essentially zero, have a value for η_E that can be used in Eq. 10, but $\mu_{\delta\widetilde{W}}$ will be nearly zero.

In our approach, we considered the uncertainty associated with the selection of a given GMM and spatial correlation model based on relationships developed by Brandenberg and Pretell (2024). Accounting for these sources of uncertainty, the ground motion *IM* for an event i at a site j was calculated using Eq. 11.

$$\mu_{\tilde{Y},ij} = \sum_{\ell=1}^{N_{GMM}} w_\ell \cdot \mu_{\hat{Y},ij\ell} + \sum_{\ell=1}^{N_{GMM}} w_\ell \cdot \eta_{E,i\ell} + \sum_{\ell=1}^{N_{GMM}} \sum_{k=1}^{N_{sample}} w_\ell \cdot w_k \cdot \mu_{\delta\widetilde{W},ijk\ell} \tag{11}$$

where w_ℓ and w_k are the weights assigned to particular GMMs and spatial correlation models, respectively, N_{GMM} is the number of GMMs considered for a given case history according to Table 2, and $N_{sample}$is the number of spatial correlation models (taken as N_{sample} = 1000). The variance was calculated using Eq. 12.

$$\sigma^2_{\tilde{Y},ij} = \sum_{\ell=1}^{N_{GMM}} \sum_{k=1}^{N_{sample}} w_\ell \cdot w_k \cdot \sigma^2_{\delta\widetilde{W},ijk\ell} + \sum_{\ell=1}^{N_{GMM}} \sum_{k=1}^{N_{sample}} w_\ell \cdot w_k \cdot \left(\mu^2_{\delta\widetilde{W},ijk\ell} - \mu^2_{\delta\widetilde{W},ij\ell}\right) + \sum_{\ell=1}^{N_{GMM}} w_\ell \cdot \left(\mu^2_{\tilde{Y},ij\ell} - \mu^2_{\tilde{Y},ij}\right) \tag{12}$$

where $\sigma_{\delta\widetilde{W},ijk\ell}$ is the standard deviation computed from Kriging interpolation for event i and site j using a spatial correlation model k, developed based on a GMM ℓ. The remaining two mean terms in Eq. 12 are defined in Eqs. 13 and 14.

$$\mu_{\delta\widetilde{W},ij\ell} = \sum_{k=1}^{N_{sample}} w_k \cdot \mu_{\delta\widetilde{W},ijk\ell} \tag{13}$$

$$\mu_{\tilde{Y},ij\ell} = \mu_{\hat{Y},ij\ell} + \eta_{E,i\ell} + \mu_{\delta\widetilde{W},ij\ell} \tag{14}$$

The term $\mu_{\delta\widetilde{W},ij\ell}$ is the weighted average within-event residual estimated from all the spatial correlation models and a given GMM ℓ, and $\mu_{\tilde{Y},ij\ell}$ is the corresponding mean ground motion *IM*, calculated considering all the spatial correlation models and a given GMM ℓ. The weights w_k and w_ℓ in Eqs. 10 to 14 reflect our judgment regarding the accuracy of the spatial correlation model realizations, and the GMMs. For the spatial correlation models, we used

1000 realizations with equal weight, w_k = 1/1000. The weights for the GMMs, w_ℓ, were selected in consideration of their nonlinear site response terms for low V_{S30}, which is a crucial model component for this application (Pretell et al. 2024b). ASK14 and CB14 used results of ground response simulations (Kamai et al. 2014) with relatively generic modulus reduction and damping curves to constrain their nonlinear models, whereas BSSA14 and CY14 considered both those same simulations and trends from interpreted ground motion data. We preferred models with data constraints of the nonlinear site response and therefore adopted w_ℓ values of 1/6, 1/6, 1/3, and 1/3 for ASK14, CB14, BSSA14, and CY14, respectively. As with the NGA-West2 GMMs, the NGA-Sub GMMs have nonlinear site response models derived using different methods. AG22 and KBCG23 use nonlinear site response models derived from equivalent-linear simulations (Walling et al. 2008), whereas PSBAH22 use a nonlinear model from Parker and Stewart (2022) that is derived from a combination of simulations (Kamai et al. 2014) and analysis of data from subduction events. We assign w_ℓ values of 1/3, 1/6, and 1/2 to the AG22, KBCG23, and PSBAH22 GMMs, respectively.

Each of the terms on the right side of Eq. 12 represents different sources of uncertainty in the interpolated ground motion *IM*s and are quantified as variances. The first term in Eq. 12 represents the uncertainty in the mean ground motion *IM* given by (1) the Kriging interpolation error for the NGL site location, (2) the standard error in the event term due to sampling error ($\bar{\tau}$), and (3) the within-event standard deviation given by GMMs (ϕ). The Kriging interpolation error has a maximum value of $\sqrt{\phi^2 + \bar{\tau}^2}$ when $\rho_{EA} = 0$ (i.e., when d_E and d_A or both are large), and decreases as the Euclidean and azimuthal distances between the NGL site and the nearest seismic station decrease. The second term in Eq. 12 represents the uncertainty associated with the interpolated mean of within-event residuals given by the different spatial correlation model coefficients computed for each of the considered GMMs (Table 2). The third term in Eq. 12 represents uncertainties in mean interpolated ground motion *IM*s from different GMMs.

Fig. 4 presents the values for the three terms in Eq. 12 for all case history *PGA*s computed using Kriging interpolation. The values are sorted by earthquake year from left to right, and for each year, increasing total uncertainty. Three values are provided for each case history corresponding to the first, second, and third terms in Eq. 12. The first term contributes most strongly to the total uncertainty in our estimated ground motion *IM*s. There is a general trend of decreasing first- and second-term uncertainties with time, which is due to the increased numbers of available earthquake recordings in more recent events. A larger number of recordings leads to (1) shorter average separation distances between NGL and ground motion measurement sites, (2) lower event term standard errors, and

(3) narrower distributions for the spatial correlation model coefficients. Factors (1) and (2) reduce first-term uncertainties, while factor (3) reduces second-term uncertainties.

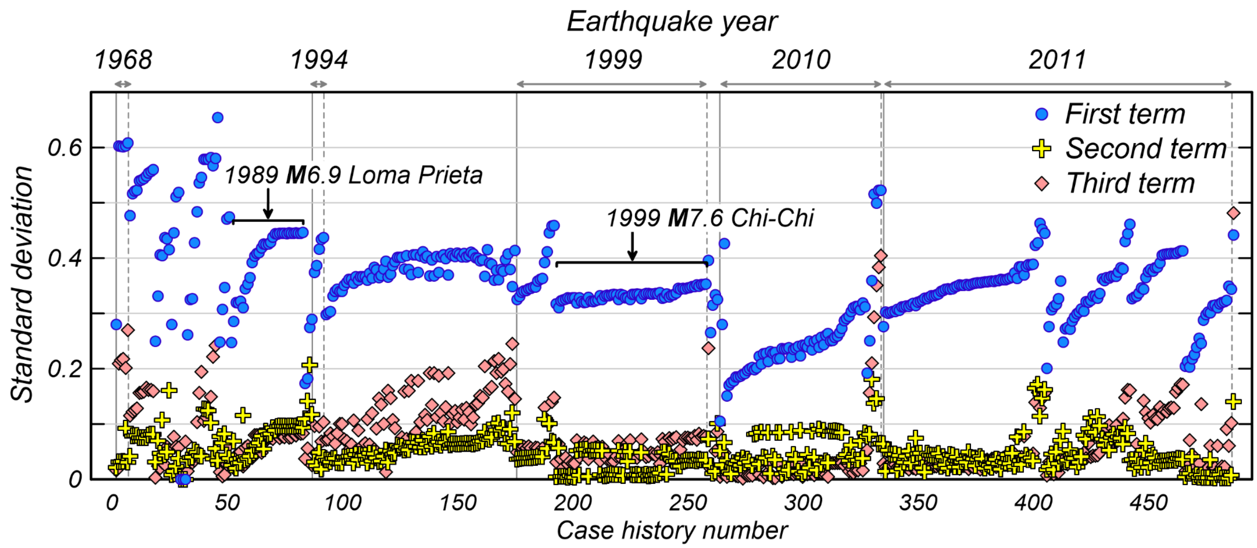

Fig. 4. Values for each of the three uncertainty components associated with interpolated *PGA*s at NGL case history sites, as defined by the three terms in Equation 12.

Fig. 4 highlights uncertainties associated with NGL sites for the 1989 Loma Prieta and the 1999 Chi-Chi Earthquakes. The first term in Eq. 12 ranges from 0.25 to 0.44 natural logarithmic units for Loma Prieta NGL sites and from 0.31 to 0.35 natural logarithmic units for Chi-Chi NGL sites. The relatively large range for Loma Prieta sites as compared to Chi-Chi is due to wider ranges of site-to-station Euclidean distances, which are 0.2 to 15.4 km for Loma Prieta, and from 0.35 to 3.2 km for Chi-Chi. Both first- and second-term uncertainties are generally lower for Chi-Chi than for Loma Prieta sites because of the differences in available recordings (161 vs. 36, respectively). Third term uncertainties are comparable for the two events.

The uncertainty associated with alternate GMMs was not evaluated for the single eastern U.S. case history, nor for I_A or *CAV* for all NGL sites. For stable continental regions, the NGA-East Gea21 reference rock GMM was used with the linear site response model for *PGA* and *PGV* by Stewart et al. (2020), the nonlinear site response model by Hashash et al. (2020), and the bias adjustment factor by Ramos-Sepúlveda et al. (2024). For I_A and *CAV*, the GMM by Farhadi and Pezeshk (2020) was used for this single site. Lastly, for active tectonic regions, the GMM by Campbell and Bozorgnia (2019) was used for I_A and *CAV*, whereas for subduction regions and earthquakes in Japan (all event types), the GMM by Foulser-Piggott and Goda (2015) was used for I_A and *CAV*. Because a single model was used in these cases, the uncertainty associated with GMM selection was not evaluated.

Though not presented here for brevity, Pretell et al. (2024) conducted a leave-one-out cross-validation for three events and showed that the results are unbiased. The values predicted at recorded locations (without considering that recording) compared reasonably well to the recorded values, with a larger discrepancy when the correlation to the nearest station was low or near zero.

Comparisons of PGA estimates at NGL sites

The newly computed *PGA*s are compared to those from previous studies (e.g., Moss 2003, Boulanger and Idriss 2014, Cetin et al. 2018) to assess the influence of the proposed methodology on *IM*s at legacy case history sites. Fig. 5 compares *PGA*s for NGL sites from the 1989 **M**6.9 Loma Prieta Earthquake. Each data point corresponds to $\mu_{\tilde{Y},ij}$ in Eq. 11 (arithmetic units) and is shown with $\pm\sigma_{\tilde{Y},ij}$ (Eq. 12) in the horizontal direction for the interpolated *IM*s. For cases where standard deviations of legacy estimates are available, bars are also presented in the vertical direction. In Fig. 5, the *RotD50* component (Boore 2010) is considered for the newly estimated *PGA*s whereas the geometric mean was generally used for legacy *PGA*s. The markers in Fig. 5 indicate the different methods used in estimating the legacy *PGA*s, which are listed in Table 1.

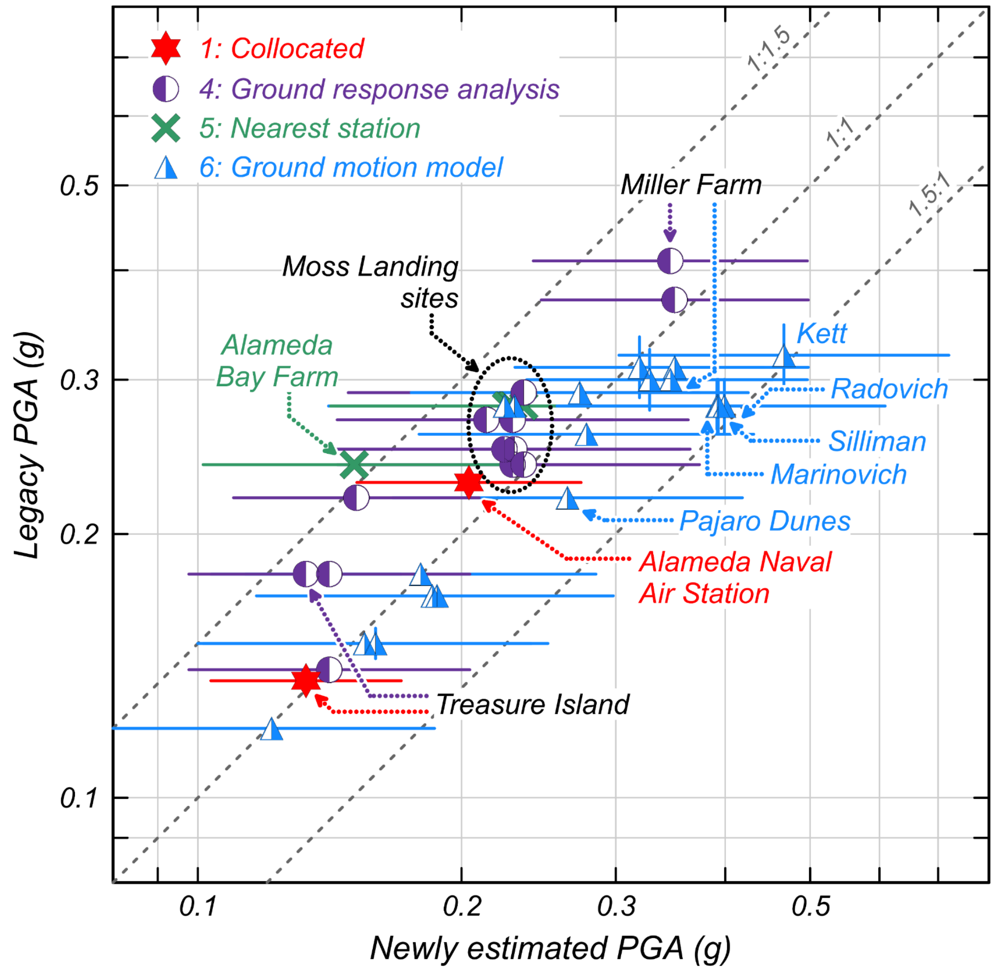

Fig. 5. Legacy versus newly estimated *PGA*s for NGL case history sites of the 1989 **M**6.9 Loma Prieta Earthquake.

The legacy *PGA*s for the Loma Prieta case history sites in Fig. 5 were based on four methods: Collocated recording (Method 1), 1D ground response analysis (Method 4), ground motions recorded at the nearest seismic station (Method 5), and GMMs (Method 6). Overall, the newly estimated and legacy *PGA*s for Loma Prieta are effectively unbiased as a population (mean difference in natural logarithmic units of -0.05) and are within a factor of 1.5 of each other, as indicated by the dashed lines in Fig. 5. A few key observations for the Loma Prieta case histories are discussed below.

The legacy *PGA*s based on collocated recordings (Method 1) correspond to the Treasure Island and Alameda Naval Air Station NGL sites. The newly estimated and legacy *PGA*s for Treasure Island are nearly the same, although with a relatively wide range along the horizontal axis (Fig. 5). The closest station was considered as "collocated" in legacy studies, however the distance to the liquefaction site is 200 m, where the *PGA* spatial correlation has dropped below 1.0 (Fig. 3d and 3e), and the Kriging standard deviation has increased from null (at zero distance) to 0.25 natural logarithmic units. The same explanation applies to the Alameda Naval Air Station site, whose *PGA* was informed by a station with similar V_{S30} located 0.5 km away, thus with a low correlation, but was judged to be collocated in past studies. The legacy *PGA*s based on ground response analysis (Method 4) are relatively close to the 1:1 line, although a few sites located in the Bay Area have newly estimated *PGA*s between 0.13 to 0.15g, which are lower than their legacy counterparts.

Legacy *PGA*s based on the nearest seismic stations (Method 5) were derived for eight cases, seven of which are sites in the Moss Landing area (indicated by the dotted oval Fig. 5). Past studies adopted a *PGA* of 0.28g for the Moss Landing sites based on a ground motion recording at the Salinas – John & Work seismic station, located about 20 km southeast of the sites, and adjusted using the Boore et al. (1993) GMM to account for differences in path and site effects. Our estimates are slightly lower, with *PGA*s ranging from 0.22 to 0.24g. The remaining site is the Alameda Bay Farm Island, whose legacy *PGA* was assigned as 0.24g based on the ground motion recorded at the Alameda Naval Air Station, located 7 km north of this site (Fig. 2). The Alameda Farm Island site is located approximately at a R_{JB} distance of 65 km, in a zone of overall underprediction by BSSA14 (Fig. 2). The relatively large distance from the fault leads to GMM-based estimates of 0.08g to 0.09g, which is increased to 0.14 to 0.16g when accounting for the interpolated within-event residuals and the event terms. At this site, the mean *PGA* resulting from Eq. 10 is approximately 0.15g.

Larger discrepancies are observed between our *PGA*s and legacy values from GMMs (Method 6), with a tendency for legacy *PGA*s to be lower. The NGL sites Kett, Silliman, Radovich, and Marinovich are located near the southern end of the fault (Fig. 2) and exhibit the most significant discrepancy (lying near the 1.5:1 line in Fig. 5). Their legacy *PGA*s were estimated by Toprak et al. (1999) who used a version of the Boore et al. (1993) GMM, that was adjusted to align with the recordings at the Watsonville and the Salinas – John & Work seismic stations. The discrepancies between Toprak et al. (1999)'s estimates and our *PGA*s are likely due to different treatment of site response in the GMMs. The Boore et al. (1993) GMM used site class as a predictor variable instead of V_{S30} and did not consider nonlinear site response effects, whereas Boore et al. (2014) used V_{S30} and includes a nonlinear site term. The net effect in these cases is ground motion increase.

Fig. 6 compares the legacy and newly estimated *PGA*s for all NGL sites as of this writing, differentiated by the method used for the legacy *PGA*s (Table 1). The reasons behind the discrepancies between legacy and newly estimated *PGA*s depend on specific aspects of the NGL sites, such as the ground motion data or site characterization used for the *PGA* estimation, the GMMs available, and judgment applied by the analysts in the legacy studies. We describe here the four most common reasons for the discrepancies. Pretell et al. (2024b) present a more detailed description by method, with a specific explanation for sites showing a legacy versus newly computed *PGA* discrepancy beyond a factor of 2.

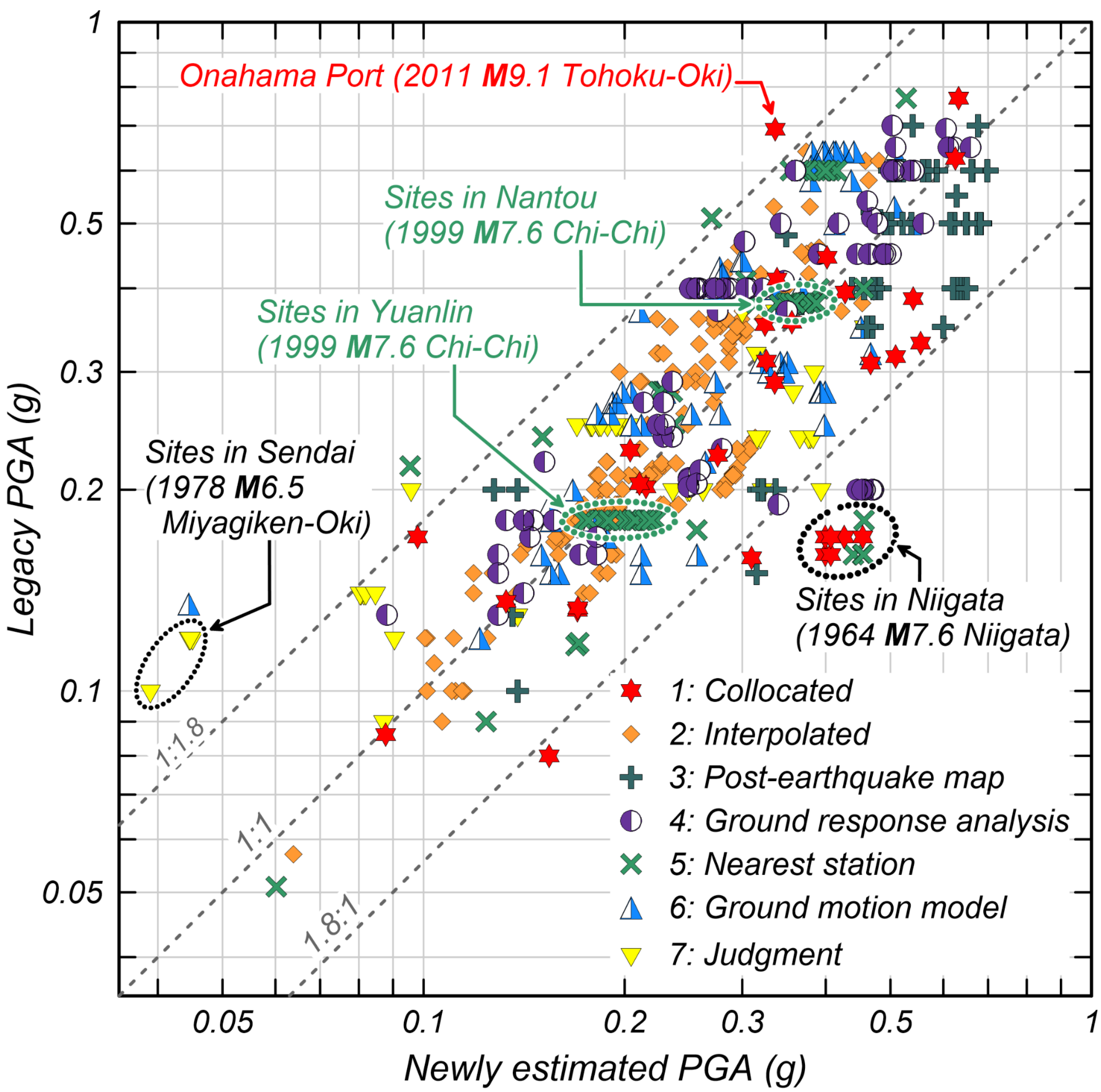

Fig. 6. Legacy versus newly estimated *PGA*s for all NGL case history sites.

Reason 1: Ground motion recordings excluded due to liquefaction effects. Our computed ground motion *IM*s are intended for use in liquefaction triggering model development, which requires that ground motions be unaffected by porewater pressure increase or the onset of liquefaction (e.g., Youd et al. 2001). Therefore, we removed recordings identified as being affected by liquefaction by Özener et al. (2020), except for the Treasure Island and the Alameda Naval Air Station recordings (1989 Loma Prieta), and the Kushiro Port recording (1993 **M**7.6 Kushiro-Oki Hokkaido Earthquake), as liquefaction triggered late in these recordings, and did not affect *PGA*. Removing these recordings led to *PGA* discrepancies for case histories whose legacy *PGA*s were based on a collocated recordings (Method 1). An example is the Onahama Port site from the 2011 **M**9.1 Tohoku-Oki Earthquake (Fig. 6). For this site, the recorded ground motions exhibited dilation spikes that led to *PGA* being significantly higher than expected if liquefaction had not occurred. Other affected sites are the Higashi-Kobe bridge, Port Island, and Kobe JI-S, from the 1995 **M**6.9 Kobe Earthquake, and several sites from the 1964 **M**7.6 Niigata Earthquake (Fig. 6).

Reason 2: Distance between measurement location and NGL site. Legacy *PGA*s were often taken from the closest seismic station (Method 5), even if such stations were located several kilometers away. The discrepancies between the legacy and newly estimated *PGA*s are due to differences in path and site effects between the NGL site and seismic station. Reason 2 focuses on path differences whil Reason 3 focuses on the effects of different site conditions. Legacy *PGA*s estimated using Method 5 often plot as a horizontal series of points in Fig. 6, corresponding to various NGL sites that had been assigned the same legacy *PGA*. Examples of such cases include various sites in Yuanlin (Taiwan) that were assigned a *PGA* of 0.18g, based on the recordings from the TCU-110 seismic station during the 1999 **M**7.6 Chi-Chi Earthquake. The R_{JB} distance for the Yuanlin sites ranges from 8 to 12.5 km, whereas the seismic station is located at a R_{JB} of 11.6 km. Our results indicate that the ground motion recorded at the TCU-110 station underestimated the *PGA*s at some liquefaction sites, which have now been assigned *PGA*s between 0.16 and 0.2g. In these cases, the site conditions are similar so the *PGA* differences mainly arise due to different paths.

Reason 3: Inconsistencies in site conditions. Differences between V_{S30} values for NGL sites and recording sites constitute the third reason for discrepancies. The differences in V_{S30} can be significant, particularly for strongly shaken soft sites, where nonlinear effects are appreciable. Two main groups are identified. First, legacy *PGA*s based on the nearest seismic station (Method 5) were often assigned to liquefaction sites despite significant differences in V_{S30}.

Examples include the Nantou sites from the 1999 **M**7.6 Chi-Chi Earthquake, which are located on young alluvial deposits with V_{S30} values between 190 and 290 m/s (Chu et al. 2004) and were assigned a *PGA* of 0.38g based on the TCU-076 station (Fig. 6). This station is located within 3 km of all NGL sites but has V_{S30} = 570 m/s. Second, multiple NGL sites in New Zealand were assigned *PGA*s computed from an interpolation approach similar to that applied herein (Method 2), but were derived from the Bradley (2013) GMM and the spatial correlation model by Goda and Hong (2008). The legacy *PGA*s for these sites were read off *PGA* maps (B. Bradley, *personal communication*, 2024) prepared for a uniform V_{S30} by Bradley and Hughes (2012) and Bradley (2014). In contrast, our *PGA* valus are based on site-specific V_{S30} based on site investigation data. These differences produce relatively small *PGA* discrepancies for various NGL sites in Christchurch from the 2010 **M**7.0 Darfield Earthquake, the 2011 **M**6.2 Christchurch Earthquake (02/21) and its 2011 **M**5.0 aftershock, the 2011 **M**6.0 Christchurch Earthquake (06/13), and 2011 **M**5.9 Lyttelton Earthquake.

Reason 4: Legacy estimates based on judgement. The causes of discrepancies observed between legacy *PGA*s and newly estimated *PGA*s are not well understood when judgment was employed in the legacy *PGA* estimation (Method 7 in Table 1) as such judgment was generally not documented and therefore cannot be replicated. Examples include the discrepancies observed for four NGL sites located in Sendai (Fig. 6) with observations from the 1978 **M** 6.5 Miyagiken-Oki Earthquake.

Impact on liquefaction triggering curves

In this section, we investigate how the updated *PGA*s impact the position of the "liquefaction" and "no liquefaction" cases in penetration resistance versus cyclic stress demand space. We use the liquefaction case histories by Idriss and Boulanger (2010) and Boulanger and Idriss (2012) that used SPT, hereafter referred to as IB10, and the case histories by Boulanger and Idriss (2014, 2016) that used CPT, hereafter referred to as BI14. Not all of the case histories considered by IB10 and BI14 are currently in the NGL database, as explained by Pretell et al. (2024b). Fig. 7 shows $(N_1)_{60cs}$ and q_{c1Ncs} versus $CSR_{M=7.5,\sigma'_v=1}$ (Eq. 1) for the IB10 SPT dataset (Fig. 7a), the BI14 CPT dataset (Fig. 7c), and those estimated in this study (Figs. 7b and 7d). The only causes of differences in $CSR_{M=7.5,\sigma'_v=1}$ between legacy values and this study are their *PGA*s.

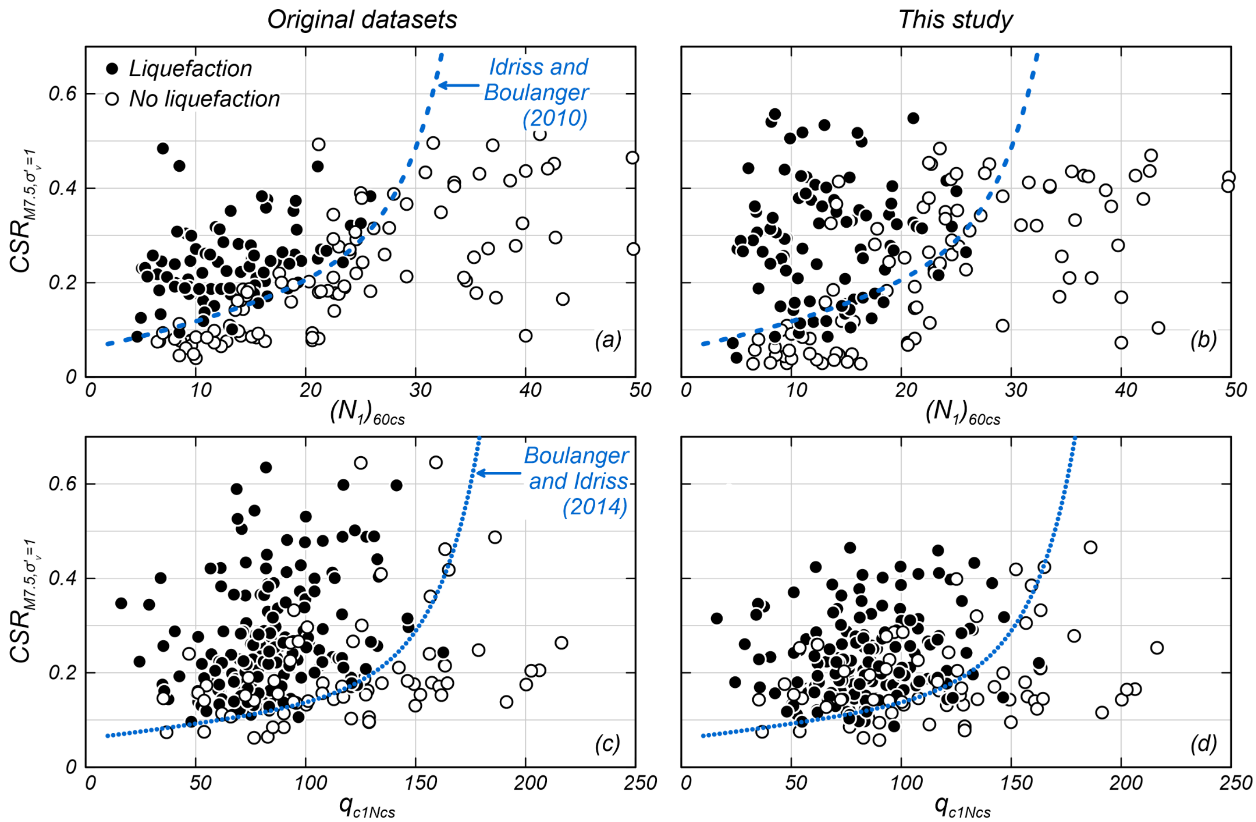

Fig. 7. Separability of liquefaction and no liquefaction cases given by Idriss and Boulanger (2010) (top row, left column) and Boulanger and Idriss (2014) (bottom row, left column), versus this study (right column): (a) and (b) show the corrected cyclic stress ratio ($CSR_{M=7.5,\sigma'_v=1}$) versus corrected standard penetration test blow counts $(N_1)_{60cs}$, and (c) and (d) show the $CSR_{M=7.5,\sigma'_v=1}$ versus corrected cone penetration test tip resistance (q_{c1Ncs}).

Fig. 7 shows that the $CSR_{M=7.5,\sigma'_v=1}$ values from this study are shifted compared to the values of IB10 and BI14. Although there is significant overlap of the "yes" and "no" liquefaction points in both datasets, the degree of overlap is greater using our *PGAs*. The SPT dataset by IB10 yields five "liquefaction" cases that plot below the liquefaction triggering model (false negatives), and 20 "no liquefaction" cases above the model (false positives), while our estimates yield 18 false negatives and 23 false positives. Meanwhile, the CPT dataset by BI14 yields five false negatives and 31 false positives, while our estimates yield 12 false negatives, and 29 false positives. The IB10 and BI14 liquefaction triggering models were not developed based on our *PGA*s, and thus a higher number of false negatives is expected. However, we report these counts to quantify the impact of our *PGA*s on existing liquefaction triggering models. If the increase in overlap of data given by our *PGA*s were to be considered in model development, larger uncertainties in the positions of liquefaction triggering curves would likely be identified.

Another observation in Fig. 7 is that our $CSR_{M=7.5,\sigma'_v=1}$ values are generally higher than those in the IB10 dataset, and lower than those in the BI14 dataset. The increase of $CSR_{M=7.5,\sigma'_v=1}$ in the SPT dataset and decrease in the CPT dataset reflect the particular conditions that are present; they are not a consequence of different underlying approaches (the same approach was applied to both the SPT and CPT datasets).

The *PGA* and other ground motion *IM*s considered in this study are presented in Fig. 8 for the CPT dataset. The observed overlap of the "yes" and "no" liquefaction data points is greater for all four intensity measures than indicated in Fig. 7 for $CSR_{M=7.5,\sigma'_v=1}$. This is expected given that important features of behavior are missing when *PGA* or other ground motion *IM*s are used on their own without earthquake magnitude or depth corrections. Comparatively, *PGA* and *PGV* render slightly less overlap than I_A and *CAV*. It is difficult to draw conclusions from these results regarding the efficiency of these *IM*s because we did not account for depth-variations, σ_v and σ'_v, or earthquake magnitude scaling. Accounting for such factors may improve separability between the "yes" and "no" points in these alternate *IM* datasets.

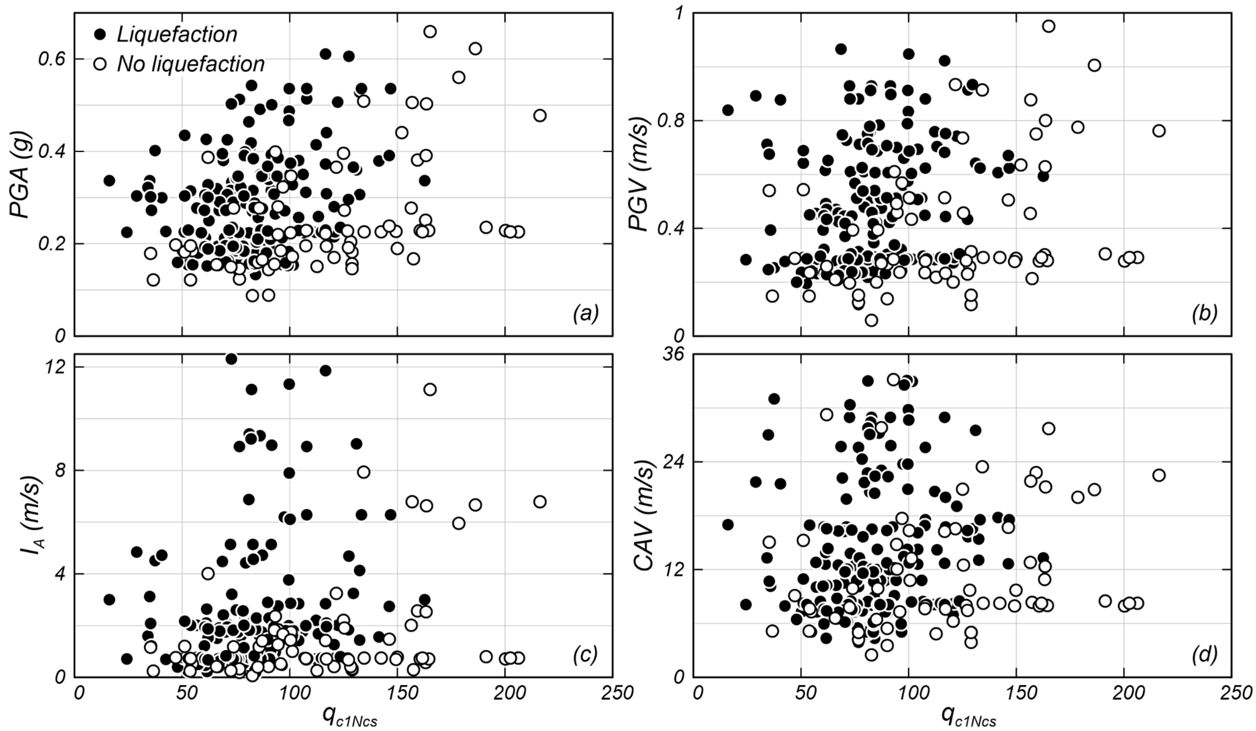

Fig. 8. Separability of liquefaction and no liquefaction cases in the seismic demand versus corrected tip resistance (q_{c1Ncs}) space. Ground motion intensity measures computed in this study for the Boulanger and Idriss (2014) case history sites: (a) Peak ground acceleration (*PGA*), (b) peak ground velocity (*PGV*), (c) Arias intensity (I_A), and (d) cumulative absolute velocity (*CAV*).

Conclusions

We computed ground motion intensity measures (*IM*s) at 569 Next Generation Liquefaction (NGL) case history sites. We adopted a framework from previous studies that overcomes various problems and inconsistencies associated with the methods used to estimate some legacy ground motion *IM*s at liquefaction case history sites. For events with ground motion recordings, our framework computes ground motion *IM*s at liquefaction sites based on ordinary Kriging and event-specific spatial correlation models developed using a Bayesian approach. This framework captures different sources of uncertainty including: (1) Kriging interpolation error associated with the event-specific spatial distribution of ground motion recordings and separation distances between NGL sites and measurement locations, (2) the event term standard error (i.e., sampling error), and (3) the within-event standard deviation from ground motion models. For most NGL sites, we find that the first of these contributors controls the uncertainty in the ground motion *IM*s. We computed peak ground acceleration (*PGA)*, peak ground velocity (*PGV*), Arias intensity (I_A), and cumulative absolute velocity (*CAV*) at 569 case history sites in the NGL database.

The differences between the new and legacy *PGA*s are small for the overall population of NGL sites (mean discrepancy of -0.034 natural logarithmic units, indicating that the new *PGA*s are 3.3% smaller), but significant differences occur for individual sites, with the spread of the *PGA* ratios being 0.5 to 2. The reasons for these differences can be grouped into four broad categories:

1. The removal of ground motion recordings affected by liquefaction effects from seismic stations collocated to liquefaction sites
2. Differences in path effects between liquefaction sites and the closest seismic station that were often unaccounted for in legacy studies
3. Differences in site conditions (i.e., different time-average shear wave velocity in the upper 30 m, V_{S30}, values) between liquefaction sites and ground motion recording sites; such differences were encountered for legacy sites where *PGA* was assigned based on the closest seismic station or *PGA* maps developed for a constant V_{S30}
4. Reasons that are not well understood when legacy *PGA*s were estimated using judgment, the basis of which was not well-documented

We also investigated how well the new *IM*s separate data points for the Idriss and Boulanger (2010) and Boulanger and Idriss (2014) standard and cone penetration test datasets, respectively. The $CSR_{M=7.5,\sigma'_v=1}$ values computed based on our *PGA*s render a slightly less clear separation of the cases of liquefaction and no liquefaction compared to the *PGA*s used by Idriss and Boulanger (2010) and Boulanger and Idriss (2014). The increased overlap of the data using the proposed ground motions would increase model uncertainty if it were considered in model development.

In addition to *PGA*, we estimated *PGV*, I_A, and *CAV* to facilitate future liquefaction triggering model development. However, several correction factors are required for their application, which is not addressed herein. As shown in Eq. 1, existing liquefaction triggering models use the *PGA* at ground surface, accompanied by a shear stress reduction factor (r_d) to account for the fact that the soil is a deformable body. Furthermore, correction factors to adjust

CSR or *CRR* to a standard **M** = 7.5 (magnitude scaling factor, *MSF*), and an overburden correction factor to a vertical effective stress of 1 atm (K_σ) are also required for some of these ground motion *IM*s. Future studies should focus on developing these correction factors for *IM*s other than *PGA*.

Data availability statement

Some or all data, models, or code generated or used during the study are available in online repositories. The ground motion intensity measures, spatial correlation models, and gmKriger (Pretell 2026), a Python-based implementation that allows the estimation of ground motion *IM*s for case history sites, are all accessible via the DesignSafe data repository at https://www.designsafe-ci.org (Pretell et al. 2023). The legacy and newly estimated ground motion *IM*s are accessible at the Next Generation Liquefaction (NGL) database (Brandenberg et al. 2020, Ulmer et al. 2023). The codes developed as part of this study are accessible via GitHub at https://github.com/RPretellD (Pretell 2025, 2026a, and 2026b). The GMM calculations were conducted using the Python-based implementations by Kottke et al. (2023), Pretell (2026), and by Dr. Silvia Mazzoni for the subduction events using the NGA-Sub database (Mazzoni et al. 2022).

Acknowledgments

The study benefitted from interactions and discussions with Dr. Kristin J. Ulmer, Prof. Paolo Zimmaro, Prof. Steven L. Kramer, Tom Shantz, and Dr. AnhDan Le. Our study built on the work by Dr. Kenneth S. Hudson (Hudson et al. 2023), and discussions with Dr. Hudson are greatly appreciated. Prof. Yousef Bozorgnia provided access to ground motion recordings from the NGA-West2 and NGA-Sub ground motion databases, and Dr. Silvia Mazzoni facilitated the computation of ground motion intensity measures using the ground motion recordings in these databases. The efforts Dr. Tristan E. Buckreis put into process ground motions for the **M**6.1 Emilia Earthquake are appreciated. The research presented in this study was sponsored by the California Department of Transportation (Caltrans) through the UCLA John B. Garrick Institute for the Risk Sciences (GIRS) under Task Order 3 through contract number 65A0780. Any opinions, findings, and conclusions expressed in this article are those of the authors and do not necessarily reflect the views of acknowledged individuals, Caltrans or GIRS.

References

Abrahamson, N. A., and Z. Gülerce. 2022. "Summary of the Abrahamson and Gülerce NGA-SUB ground-motion model for subduction earthquakes." Earthquake Spectra, 38(4), 2638–2681. https://doi.org/10.1177/87552930221114374.

Abrahamson, N. A., W. J. Silva, and R. Kamai. 2014. "Summary of the ASK14 ground motion relation for active crustal regions." Earthquake Spectra, 30(3), 1025–1055. https://doi.org/10.1193/070913EQS198M.

Abrahamson, N. A., and R. R. Youngs. 1992. "A stable algorithm for regression analyses using the random effects model." Bulletin of the Seism. Society of America, 82(1), 505–510. https://doi.org/10.1785/BSSA0820010505.

Ahdi, S. K., D. Y. Kwak, T. D. Ancheta, V. Contreras, T. Kishida, A. O. Kwok, S. Mazzoni, F. Ruz, and J. P. Stewart. 2022. "Site parameters applied in NGA-Sub database." Earthquake Spectra, 38(1), 494–520. https://doi.org/10.1177/87552930211043536.

Ancheta, T. D., R. B. Darragh, J. P. Stewart, E. Seyhan, W. J. Silva, B. S.-J. Chiou, K. E. Wooddell, R. W. Graves, A. R. Kottke, D. M. Boore, T. Kishida, and J. L. Donahue. 2014. "NGA-West2 database." Earthquake Spectra, 30, 989–1005. https://doi.org/10.1193/070913EQS197M.

Andrus, R. D., N. P. Mohanan, P. Piratheepan, B. S. Ellis, and T. L. Holzer. 2007. "Predicting shear-wave velocity from cone penetration resistance." In Proc., 4th Int. Conf, on Earthquake Geotechnical Eng., Thessaloniki, Greece.

Bodenmann, L., J. W. Baker, and B. Stojadinovic. 2023. "Accounting for path and site effects in spatial ground-motion correlation models using Bayesian inference." Natural Hazards and Earth System Sciences, 23, 2387–2402. https://doi.org/10.5194/nhess-23-2387-2023.

Boore, D. M. 2004. "Estimating V_{S30} (or NEHRP Site Classes) from shallow velocity models (Depths < 30 m)." Bulletin of the Seismological Society of America, 94(2), 591–597. https://doi.org/10.1785/0120030105.

Boore, D. M. 2010. "Orientation-independent, nongeometric-mean measures of seismic intensity from two horizontal components of motion." Bulletin of the Seismological Society of America, 100(4): 1830–1835. https://doi.org/10.1785/0120090400.

Boore, D. M., W. B. Joyner, and T. E. Fumal. 1993. Estimation of the response spectra and peak accelerations from western North American earthquakes: An interim report. US Geological Survey, Open-file Report 95-663, 357.

Boore, D. M., J. P. Stewart, E. Seyhan, and G. M. Atkinson. 2014. "NGA-West2 equations for predicting PGA, PGV, and 5% damped PSA for shallow crustal earthquakes." Earthquake Spectra, 30(3), 1057–1085. https://doi.org/10.1193/070113EQS184M.

Boulanger, R. W., and I. M. Idriss. 2012. "Probabilistic standard penetration test-based liquefaction-triggering procedure." Journal of Geotechnical and Geoenvironmental Engineering, 138(10): 1185–1195. https://doi.org/10.1061/(ASCE)GT.1943-5606.0000700.

Boulanger, R. W., and I. M. Idriss. 2014. CPT and SPT based liquefaction triggering procedures. Report No. UCD/CGM-14/01, Center for Geotechnical Modeling, Dept. Civil and Environmental Eng., UC Davis.

Boulanger, R. W., and I. M. Idriss. 2016. "CPT-based liquefaction triggering procedure." Journal of Geotechnical and Geoenvironmental Engineering, 142(2): 04015065. https://doi.org/10.1061/(ASCE)GT.1943-5606.0001388.

Bradley, B. A. 2013. "A New Zealand-specific pseudo-spectral acceleration ground motion prediction equation for active shallow crustal earthquakes based on foreign models." Bulletin of the Seism. Society of America, 103(3), 1801–1822. https://doi.org/10.1785/0120120021.

Bradley, B. A. 2014. "Site-specific and spatially distributed ground-motion intensity estimation in the 2010-2011 Canterbury earthquakes." Soil Dynamics Earthquake Engineering, 61(2014), 83–91. https://doi.org/10.1016/j.soildyn.2014.01.025.

Bradley, B. A., and M. Hughes. 2012. Conditional Peak Ground Accelerations in the Canterbury Earthquakes for Conventional Liquefaction Assessment. Technical Report prepared for the Dept. of Building and Housing.

Brandenberg, S. J., N. Bellana, and T. Shantz. 2010. "Shear wave velocity as a function of standard penetration test resistance and vertical effective stress at California bridge sites." Soil Dynamics and Earthquake Engineering, 30(10), 1026–1035. https://doi.org/10.1016/j.soildyn.2010.04.014.

Brandenberg, S. J., and R. Pretell. 2024. "Evaluating epistemic uncertainty from random variables at the terminal branches of a logic tree." Journal of Risk and Uncertainty in Eng. Systems, Part A: Civil Engineering 10(3): 06024003. https://doi.org/10.1061/AJRUA6.RUENG-1267.

Brandenberg, S. J., P. Zimmaro, J. P. Stewart, D. Y. Kwak, K. W. Franke, R. E. S. Moss, K. O. Cetin, G. Can, M. Ilgac, J. Stamatakos, T. Weaver, and S. L. Kramer. 2020. "Next-Generation Liquefaction database." Earthquake Spectra, 36(2), 939–959. https://doi.org/10.1177/8755293020902477.

Buckreis, T. E., J. P. Stewart, S. J. Brandenberg, and P. Wang. 2024. "Small-strain site response of soft soils in the Sacramento-San Joaquin Delta region of California conditioned on V_{S30} and HVSR." Earthquake Spectra, 40(1), 230–260. https://doi.org/10.1177/87552930231217165.

Campbell, K. W., and Y. Bozorgnia. 2014. "NGA-West2 ground motion model for the average horizontal components of PGA, PGV, and 5% damped linear acceleration response spectra." Earthquake Spectra, 30, 1087–1115. https://doi.org/10.1193/062913EQS175M.

Campbell, K.W., and Y. Bozorgnia. 2019. "Ground motion models for the horizontal components of Arias intensity (AI) and Cumulative Absolute Velocity (CAV) using the NGA-West2 database." Earthquake Spectra, 35(3), 1289–1310. https://doi.org/10.1193/090818EQS212M.

Cetin, K. O., R. B. Seed, A. Der Kiureghian, K. Tokimatsu, L. F. Harder, R. E. Kayen, and R. E. S. Moss. 2004. "Standard penetration test-based probabilistic and deterministic assessment of seismic soil liquefaction potential." Journal of Geotechnical and Geoenvironmental Engineering, 130(12): 1314–1340. https://doi.org/10.1061/(ASCE)1090-0241(2004)130:12(1314).

Cetin, K. O., R. B. Seed, R. E. Kayen, R. E. S. Moss, T. Bilge, M. Ilgac, and K. Chowdhury. 2018. "Dataset on SPT-based seismic soil liquefaction." Data in Brief 20: 544–548. https://doi.org/10.1016/j.dib.2018.08.043.

Cetin, K. O., R. B. Seed, R. E. S. Moss, A. K. Der Kiureghian, K. Tokimatsu, L. F. Harder, and R. E. Kayen. 2000. Field case histories for SPT-based in situ liquefaction potential evaluation. Geotechnical Engineering Research Report No. UCB/GT-2000/09, Geotechnical Engineering, Dept. Civil Engineering, UC Berkeley.

Chiou, B. S.-J., and R. R. Youngs. 2014. "Update of the Chiou and Youngs NGA model for the average horizontal component of peak ground motion and response spectra." Earthquake Spectra, 30(3), 1117–1153. https://doi.org/10.1193/072813EQS219M.

Chu, D., J. P. Stewart, S. Lee, J. S. Tsai, P. S. Lin, B. L. Chu, R. B. Seed, S. C. Hsu, M. S. Yu, and C. H. Wang. 2004. "Documentation of soil conditions at liquefaction and non-liquefaction sites from 1999 Chi-Chi (Taiwan) earthquake.” Soil Dynamics and Earthquake Engineering, 24(2004), 647–657. https://doi.org/10.1016/j.soildyn.2004.06.005.

Engler, D. T., C. B. Worden, E. M. Thompson, and K. S. Jaiswal. 2022. “Partitioning ground motion uncertainty when conditioned on station data.” Bulletin of the Seismological Society of America, 112(2), 1060–1079. https://doi.org/10.1785/0120210177.

Farhadi, A., and S. Pezeshk. 2020. “A referenced empirical ground-motion model for Arias intensity and cumulative absolute velocity based on the NGA-East database.” Bulletin of the Seismological Society of America, 110, 508–518. https://doi.org/10.1785/0120190267.

Foulser-Piggott, R., and K. Goda. 2015. “Ground-motion prediction models for Arias intensity and cumulative absolute velocity for Japanese earthquakes considering single-station sigma and within-event spatial correlation.” Bulletin of the Seismological Society of America, 105(4), 1903–1918. https://doi.org/10.1785/0120140316.

Goda, K., and H. P. Hong. 2008. “Spatial correlation of peak ground motions and response spectra.” Bulletin of the Seismological Society of America, 98, 354–365. https://doi.org/10.1785/0120070078.

Goulet, C. A., Y. Bozorgnia, N. Kuehn, L. Al Atik, R. R. Youngs, R. W. Graves, and G. M. Atkinson. 2021. “NGA-East Ground-Motion Characterization model part I: Summary of products and model development.” Earthquake Spectra, 37(S1), 1231–1282. https://doi.org/10.1177/87552930211018723.

Hashash, Y. M. A., O. Ilhan, J. A. Harmon, G. A. Parker, J. P. Stewart, E. M. Rathje, K. W. Campbell, and W. J. Silva. 2020. “Nonlinear site amplification model for ergodic seismic hazard analysis in Central and Eastern North America.” Earthquake Spectra 36(1): 69–86. https://doi.org/10.1177/8755293019878193.

Hegazy, Y. A., and P. W. Mayne. 2006. “A global statistical correlation between shear wave velocity and cone penetration data.” In Proc., GeoShanghai 2006, Site and Geomaterial Characterization (GSP 149), Shanghai, China.

Hudson, K. S., S. J. Brandenberg, P. Zimmaro, K. Ulmer, S. L. Kramer, and J. P. Stewart. 2023. “Kriging interpolation of ground motion residuals at liquefaction case history sites.” In Proc., *Geo-Congress 2023,* Los Angeles, CA.

Idriss, I. M., and R. W. Boulanger. 2008. Soil Liquefaction During Earthquakes. Earthquake Engineering Research Institute, MNO-12, Oakland, California.

Idriss, I. M., and R. W. Boulanger. 2010. SPT-based liquefaction triggering procedures. Report No. UCD/CGM-10/02, Center for Geotechnical Modeling, Dept. Civil and Environmental Engineering, UC Davis.

Jayaram, N., and J. W. Baker. 2009. “Correlation model for spatially distributed ground-motion intensities.” Earthquake Engineering and Structural Dynamics, 38, 1687–1708. https://doi.org/10.1002/eqe.922.

Kamai, R., Abrahamson, N. A., and Silva, W. J. 2014. “Nonlinear Horizontal Site Amplification for Constraining the NGA-West2 GMPEs.” Earthquake Spectra 30(3): 1223–1240. https://doi.org/10.1193/070113EQS187M.

Kayen, R. E., and J. K. Mitchell. 1997. “Assessment of liquefaction potential during earthquakes by Arias intensity.” Journal of Geotechnical and Geoenvironmental Engineering, 123(12): 1162–1174. https://doi.org/10.1061/(ASCE)1090-0241(1997)123:12(1162).

Kottke, A., Lavrentiadis, G., Marafi, N., and Pretell, R. 2023. pygmm (v0.6.6). Zenodo.

Kramer, S. L., and R. A. Mitchell. 2006. “Ground motion intensity measures for liquefaction hazard evaluation.” Earthquake Spectra, 22(2), 413–438. https://doi.org/10.1193/1.2194970.

Kramer, S. L., and S. S. Sideras. 2022. “Transient loading effects on pore pressure generation and the response of liquefiable soils.” In Proc., 4th Int. Conf. Performance-Based Design in Earthquake. Geotech. Eng., Beijing, China.

Krige, D. G. 1951. “A statistical approach to some basic mine valuation problems on the Witwatersrand.” Journal of the Chemical, Metallurgical Mining Soc. South Africa, 94(3), 95–111. https://hdl.handle.net/10520/AJA0038223X_4792.

Kuehn, N. M., N. A. Abrahamson, and M. A. Walling. 2019. “Incorporating nonergodic path effects into the NGA-West2 ground-motion prediction equations.” Bulletin of the Seismological Society of America, 109(2), 575-585. https://doi.org/10.1785/0120180260.

Kuehn, N. M., Y. Bozorgnia, K. W. Campbell, and N. Gregor. 2023. “A regionalized partially nonergodic ground-motion model for subduction earthquakes using the NGA-Sub database.” Earthquake Spectra, 39(3), 1625–1657. https://doi.org/10.1177/87552930231180906.

Kwak, D. Y., A. Mikami, S. J. Brandenberg, and J. P. Stewart. 2012. “Ground motion estimation for evaluation of levee performance in past earthquakes.” In Proc., 9th Int. Conf. Urban Earthquake Engineering/4th Asia Conf. on Earthquake Eng., Tokyo, Japan.

Mazzoni, S., T. Kishida, J. P. Stewart, V. Contreras, R. B. Darragh, T. D. Ancheta, B. S.-J. Chiou, W. J. Silva, and Y. Bozorgnia. 2022. "Relational database used for ground-motion model development in the NGA-sub project." Earthquake Spectra, 38(2), 1529 – 1548. https://doi.org/10.1177/87552930211055204.

McGann, C. R., B. A. Bradley, M. L. Taylor, L. M. Wotherspoon, and M. Cubrinovski. 2015. "Development of an empirical correlation for predicting shear wave velocity of Christchurch soils from cone penetration test data." Soil Dynamics and Earthquake Engineering, 75, 66–75. https://doi.org/10.1016/j.soildyn.2015.03.023.

Moss, R. E. S. 2003. CPT-based probabilistic assessment of seismic soil liquefaction initiation. Ph.D. dissertation, UC Berkeley.

Moss, R. E. S., R. B. Seed, R. E. Kayen, J. P. Stewart, A. Der Kiureghian, and K. O. Cetin. 2006. "CPT-based probabilistic and deterministic assessment of in situ seismic soil liquefaction potential." Journal of Geotechnical and Geoenvironmental Engineering, 132(8): 1032–1051. https://doi.org/10.1061/(ASCE)1090-0241(2006)132:8(1032).

Özener, P. T., M. W. Greenfield, S. S. Sideras, and S. L. Kramer. 2020. "Identification of time of liquefaction triggering." Soil Dynamics and Earthquake Engineering, 128(2020), 105895. https://doi.org/10.1016/j.soildyn.2019.105895.

Parker, G. A., and J. P. Stewart. 2022. "Ergodic site response model for subduction zone regions." Earthquake Spectra, 38(2), 841–864. https://doi.org/10.1177/87552930211056963.

Parker, G. A., J. P. Stewart, D. M. Boore, G. M. Atkinson, and B. Hassani. 2022. "NGA-subduction global ground motion models with regional adjustment factors." Earthquake Spectra, 38(1), 456–493. https://doi.org/10.1177/87552930211034889.

Pretell, R. 2026a. geostats: A suite of geostatistical tools (0.2.0). Zenodo.

Pretell, R. 2025. gmimtools: A suite of ground motion intensity measure tools (0.2.0). Zenodo.

Pretell, R. 2026b. gmms: Ground motion models and supporting tools (0.2.0). Zenodo.

Pretell, R., Brandenberg, S., and Stewart, J. (2026). gmKriger: Kriging-based ground motion intensity measure calculator (1.0.0). 10.5281/zenodo.10399418. Zenodo.

Pretell, R., S. Brandenberg, and J. Stewart. 2023. “Consistently computed ground motion intensity measures for liquefaction triggering assessment.” DesignSafe-CI. https://doi.org/10.17603/ds2-6vj1-t096.

Pretell, R., S. Brandenberg, and J. Stewart. 2024a. “Consistent framework for PGA estimation at liquefaction case history sites: Application to the 1989 M6.9 Loma Prieta earthquake.” In Proc., Geo-Congress 2024, Geotechnics of Natural Hazards, Vancouver, BC.

Pretell, R., S. J. Brandenberg, and J. P. Stewart. 2024b. Ground motion intensity measures at liquefaction field case history sites. Report No. GIRS-2024-02, B. John Garrick Institute for the Risk Sciences.

Ramos-Sepúlveda, M. E., J. P. Stewart, G. A. Parker, M. P. Moschetti, E. M. Thompson, S. J. Brandenberg, Y. M. A. Hashash, and E. M. Rathje. 2024. “Data-driven adjustments for combined use of NGA-East hard-rock ground motion and site amplification models.” Earthquake Spectra, 40(2): 1132–1157. https://doi.org/10.1177/87552930241231825.

Robertson P.K. (2012). Interpretation of in situ tests – some insights. *J.K. Mitchell Lecture.* In Proc., ISC4, Recife, Brazil.

Salvatier J., T.V. Wiecki, and C. Fonnesbeck. 2016. “Probabilistic programming in Python using PyMC3.” *PEERJ Computer Science*, 2:e55. https://doi.org/10.7717/peerj-cs.55.

Seed, H. B., and I. M. Idriss. 1971. “Simplified procedure for evaluating soil liquefaction potential.” Journal of Soil Mechanics and Found. Div., 97(9), 1249–1273. https://doi.org/10.1061/JSFEAQ.0001662.

Seyhan, E., J. P. Stewart, T. D. Ancheta, R. B. Darragh, and R. W. Graves. 2014. “NGA-West2 site database.” Earthquake Spectra, 30(3), 1007–1024. https://doi.org/10.1193/062913EQS180M.

Stafford, P. J. 2012. “Evaluation of structural performance in the immediate aftermath of an earthquake: A case study of the 2011 Christchurch earthquake.” Int. J. Forensic Eng., 1(1), 58–77. https://doi.org/10.1504/IJFE.2012.047447.

Stewart, J. P., G. A. Parker, G. M. Atkinson, D. M. Boore, Y. M. A. Hashash, and W. J. Silva. 2020. “Ergodic site amplification model for central and eastern North America.” Earthquake Spectra, 36(1): 42–68. https://doi.org/10.1177/8755293019878185.

Toprak, S., Holzer, T. L., Bennett, M. J., and Tinsley, J. C. I. 1999. "CPT- and SPT-based probabilistic assessment of liquefaction." In Proc., 7th US-Japan Workshop on Earthquake Resistant Design of Lifelines Facilities and Countermeasures against Liquefaction, Nat. Center for Earthquake Engineering and Research, Seattle, WA.

Ulmer, K. J., P. Zimmaro, S. J. Brandenberg, J. P. Stewart, K. S. Hudson, A. W. Stuedlein, A. Jana, A. Dadashiserej, S. L. Kramer, K. O. Cetin, G. Can, M. Ilgac, K. W. Franke, R. E. S. Moss, S. F. Bartlett, M. Hosseinali, H. Dacayanan, D. Y. Kwak, J. Stamatakos, J. Mukherjee, U. Salman, S. Ybarra, and T. Weaver. 2023. Next-Generation Liquefaction Database, Version 2. Next-Generation Liquefaction Consortium.

Upadhyaya, S., R. A. Green, A. Rodriguez-Marek, B. W. Maurer, L. Wotherspoon, B. A. Bradley, and M. Cubrinovski. 2019. "Influence of Corrections to Recorded Peak Ground Accelerations due to Liquefaction on Predicted Liquefaction Response During the 2010-2011 Canterbury, New Zealand, Earthquake Sequence." In, Proc. 13th Australia New Zealand Conference on Geomechanics (13ANZCG), Perth, Australia, 1-3 April.

Walling, M., W. Silva, and N. Abrahamson. 2008. "Nonlinear site amplification factors for constraining the NGA models." Earthquake Spectra, 24(1), 243–255. https://doi.org/10.1193/1.2934350.

Worden, C. B., E. M. Thompson, J. W. Baker, B. A. Bradley, N. Luco, and D. J. Wald. 2018. "Spatial and spectral interpolation of ground-motion intensity measure observations." Bulletin of the Seismological Society of America, 108, 866–875. https://doi.org/10.1785/0120170201.

Youd, T. L., I. M. Idriss, R. D. Andrus, I. Arango, G. Castro, J. T. Christian, R. Dobry, W. D. L. Finn, L. F. Harder, M. E. Hynes, K. Ishihara, J. P. Koester, S. S. C. Liao, W. F. Marcuson, G. R. Martin, J. K. Mitchell, Y. Moriwaki, M. S. Power, P. K. Robertson, R. B. Seed, and K. H. Stokoe. 2001. "Liquefaction resistance of soils: summary report from the 1996 NCEER and 1998 NCEER/NSF workshops on evaluation of liquefaction resistance of soils." Journal of Geotechnical and Geoenvironmental Engineering, 127(10): 817–833. https://doi.org/10.1061/(ASCE)1090-0241(2001)127:10(817).